Vol 11 No 1, January 2002
1009-1963/2002/11(01)/0077-06
Chinese Physics
© 2002 Chin. Phys. Soc.
and IOP Publishing Ltd

The effect of Nb addition on the thermal stability and magnetic properties of Fe-based amorphous alloys with a wide supercooled liquid region

Rong Chuan-Bing(荣传兵)[a)b)], Zhao Yu-Hua(赵玉华)[b)], Cheng Li-Zhi(程力智)[b)],
Xu Min(徐 民)[c)], He Kai-Yuan(何开元)[b)], and Zhao Heng-He(赵恒和)[b)]

[a)] *State Key Laboratory of Magnetism, Institute of Physics & Center for Condensed Matter Physics, Chinese Academy of Sciences, Beijing* 100080, *China*

[b)] *Department of Functional Materials, Institute of Material and Metallurgy, Northeastern University, Shenyang* 110004, *China*

[c)] *State Key Laboratory of Rapidly Solidified Nonequilibrium Alloys, Institute of Metal Research, Chinese Academy of Sciences, Shenyang* 110016,*China*

(Received 18 June 2001; revised manuscript received 30 August 2001)

We have examined the effect of Nb addition on the thermal stability of the supercooled liquid before crystallization, the glass-forming ability and magnetic properties for the amorphous alloy series $Fe_{73}Nb_xAl_{5-x}Ge_2P_{10}C_6B_4$ and $Fe_{63}Co_7Nb_xZr_{10-x}B_{20}$. The supercooled liquid regions (ΔT_x=T_x–T_g) have maximum values of 66 and 79K, respectively, for $Fe_{73}Nb_1Al_4Ge_2P_{10}C_6B_4$ and $Fe_{63}Co_7Nb_4Zr_6B_{20}$ alloys. The saturation magnetization σ_s of the $Fe_{73}Nb_xAl_{5-x}Ge_2P_{10}C_6B_4$ alloy system is much higher than that of the $Fe_{63}Co_7Nb_xZr_{10-x}B_{20}$ alloy system, and is almost unchanged with an increasing Nb content from 0 to 3 at%. But the σ_s of the $Fe_{63}Co_7Nb_xZr_{10-x}B_{20}$ alloys decreases linearly with increasing Nb content. The coercive force H_c of the two alloy series can have a minimum value of 31A/m for $Fe_{73}Nb_1Al_4Ge_2P_{10}C_6B_4$ and 37A/m for $Fe_{63}Co_7Nb_4Zr_6B_{20}$. All these values are for the ribbons annealed at 773 and 873K for 15min in vacuum.

Keywords: supercooled liquid region, ferromagnetism, amorphous alloy
PACC: 7550K, 6470P, 6470D, 8120P

1. Introduction

Recently, amorphous alloys with a large glass-forming ability (GFA) have been found in multi-component alloy systems such as Mg–*Ln*–(Ni,Cu),[1,2] *Ln*–Al–*TM*,[3] Zr–Al–*TM*,[4] Zr–Ti–Al–*TM*,[5] Zr–Ti–*TM*–Be (*Ln*=lanthanide metal, *TM*=transition metal),[6] Pd–Ni–P[7,8] and Pd–Cu–Ni–P.[9,10] It has been reported that these amorphous alloys all have a supercooled liquid region ΔT_x (defined by the difference between the crystallization temperature T_x and glass transition temperature T_g) of over 60K wide, and a large critical thickness up to 72mm for samples produced by different methods,[10] such as copper mould casting,[3] water quenching,[9] flux treatment,[10] and quenching with rapid decompression,[12] etc. It has been proven by many studies that alloys, which have a wide supercooled liquid region, show a large GFA and can be made into bulk amorphous. Furthermore, Inoue[13] and Shen and Schwarz[14] have proposed three empirical rules for the achievement of large GFA: (1) a system of multi-components containing more than three elements; (2) a significant difference in atomic size, above 12%, among the main constituent elements; (3) the alloys system must contain two or more metallic elements with different atomic sizes and near-zero heats of mixing, and the metallic elements must have large negative heats of mixing with the metalloid(s).

Magnetic materials are always an important research field of nanocrystalline and amorphous alloys.[13,15–17] More recently, Inoue has succeeded in fabricating two kinds of soft ferromagnetic bulk amorphous alloys with a wide supercooled region: Fe–(Al,Ga)–(P,C,B,Si)[18] and (Fe,Co,Ni)–Zr–B.[19] The ΔT_x of these alloys can reach 60 and 68K, respectively. It is known that a highly dense random-packed structure can be formed by adding elements with high melting points into an alloy and this structure can lead to a large supercooled liquid region.[20] The dissolution of Nb is expected to cause a further increase in the thermal stability of a supercooled liquid and its GFA. In this paper we report on the thermal stability of the supercooled liquid, the GFA and magnetic properties for $Fe_{73}Nb_xAl_{5-x}Ge_2P_{10}C_6B_4$ and $Fe_{63}Co_7Nb_xZr_{10-x}B_{20}$ amorphous alloys.

2. Experimental procedure

The ingots were prepared by arc melting the mixture of pure Fe, Co, Nb, Zr, Al, Ge metals, pre-alloyed Fe–P (containing 17.5wt%P), Fe–C (containing 6.3wt%C) and Fe–B (containing 17.9wt%B) master alloys in a purified argon atmosphere. The compositions are nominally expressed in atomic per cent. Rapidly solidified ribbons with a cross section of $0.03\times5\text{mm}^2$ were prepared by melt-spinning the master ingots in an argon atmosphere. The surface velocity of the copper wheel was 25m/s. The melt-spun ribbons were annealed at 573–973K for 15min in vacuum. The X-ray diffraction data, used to determine the amorphousness of the ribbons, were obtained by a D/Max-γA diffractometer with Cu$K\alpha$ radiation. The thermal stability, associated with the glass transition temperature T_g, supercooled liquid region ΔT_x, and the crystallization temperature T_x, was examined at a heating rate of 0.67K/s with a differential scanning calorimeter (DSC) for $Fe_{73}Nb_xAl_{5-x}Ge_2P_{10}C_6B_4$ alloys and by differential thermal analysis (DTA) for $Fe_{63}Co_7Nb_xZr_{10-x}B_{20}$ alloys. The saturation magnetization σ_s at room temperature was measured in a maximum applied field of 800kA/m with a Faraday magnetic balance. The magnetostriction $(\lambda_{/\!/} - \lambda_\perp)$ and coercive force H_c were obtained by YJ-25 magnetostriction measurement and CD-4 static magnetic measurement, respectively.

3. Results and discussion

3.1. Structure and thermal stability

Figure 1 shows the X-ray diffraction patterns taken from the freely solidified surfaces of $Fe_{73}Nb_xAl_{5-x}Ge_2P_{10}C_6B_4$ and $Fe_{63}Co_7Nb_xZr_{10-x}B_{20}$ melt-spun ribbons. Only a broad peak could be seen at a wave vector ($K_p=4\pi\sin\theta/\lambda$) of about 30.24nm^{-1} and no diffraction peak corresponding to a crystalline phase was seen for all the alloys. Figure 2 shows the DSC curves of the melt-spun $Fe_{73}Nb_xAl_{5-x}Ge_2P_{10}C_6B_4$ amorphous alloys, and DTA curves of the $Fe_{63}Co_7Nb_xZr_{10-x}B_{20}$ amorphous alloys. It is noticed that a distinct glass transition, followed by a wide supercooled liquid region, is observed in the temperature range before crystallization for all the alloys. Based on the DSC and DTA curves of the $Fe_{73}Nb_xAl_{5-x}Ge_2P_{10}C_6B_4$ and $Fe_{63}Co_7Nb_xZr_{10-x}B_{20}$ alloys, as shown in Fig.2, the T_g, T_x and ΔT_x as functions of Nb content are plotted in Fig.3. From Fig.3(a), we can see that T_g increases from 743 to 757K by the dissolution of Nb, while T_x increases from 803 to 814K by dissolution of 1 at% Nb and then decreases with a further increase of Nb content for the $Fe_{73}Nb_xAl_{5-x}Ge_2P_{10}C_6B_4$ alloy system. As a result, ΔT_x shows a maximum value of 66K for the alloy containing 1 at% Nb. Figure 3(b) shows that T_g and T_x are 883 and 952K, respectively, for 0 at% Nb alloy of the $Fe_{63}Co_7Nb_xZr_{10-x}B_{20}$ series. These decrease due to the dissolution of Nb, but the decrease of T_g is larger than that of T_x for the alloys containing 0–4 at% Nb, while the decrease of T_g is much slower than that of T_x with a further increase in Nb content up to 6 at%. This leads to the increase of ΔT_x from 69K for 0 at% Nb alloy to the maximum value of 79K for 4 at% Nb alloy. Thus, the replacement of Al or Zr by a small amount of Nb is effective for the increase in the thermal stability of the supercooled liquid for these two alloy systems.

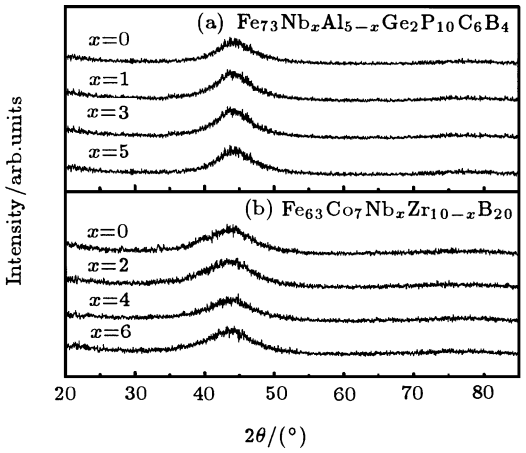


Fig.1. X-ray diffraction patterns taken from the freely solidified surfaces of $Fe_{73}Nb_xAl_{5-x}Ge_2P_{10}C_6B_4$ and $Fe_{63}Co_7Nb_xZr_{10-x}B_{20}$ melt-spun ribbons.

The remarkable increase in ΔT_x allows us to expect that the two alloy series have a large GFA that enables the production of bulk amorphous alloys by special solidification processes. Consequently, it is important to discuss the reason for the enhanced extension of the supercooled liquid region before crystallization by dissolution of Nb. The previous data[13] have indicated that the alloys following the three empirical rules can have a unique disordered structure with a higher packing density, a new local atomic configuration which is different from their crystalline phases, and a homogeneous atomic configuration on a long-range scale.[20] The wide regions of the supercooled liquids in our alloy systems are also due to

the satisfaction of the three empirical rules, as follows. (1) The alloy systems consist of seven and five constituent elements, respectively, for the two alloy series given above. (2) The atomic sizes of the $Fe_{73}Nb_xAl_{5-x}Ge_2P_{10}C_6B_4$ alloys change according to the order of Al≫Nb≫Fe>Ge≫P>B>C, and the different atomic size ratios are larger than 15% and 12%, respectively, for Nb–Fe and Fe–P pairs. In the same way, we know that the atomic size of $Fe_{63}Co_7Nb_xZr_{10-x}B_{20}$ alloys change according to the order of Zr≫Nb≫Co>Fe≫B and the different atomic size ratios are larger than 14% and 21%, respectively, for Nb–Co and Fe–B pairs. (3) The large negative heats of mixing among the main constituent elements are 22–59kJ/mol atom for Fe–Zr, Co–Zr, Fe–Al and Fe–Ge pairs; 32–60kJ/mol atom for Fe–B, Co–B, Fe–P, Co–P, Fe–C and Co–C pairs; 79–140kJ/mol atom for Zr–B, Zr–C and Zr–P pairs.[21] The addition of an appropriate amount of Nb is expected to cause an enhancement in the satisfaction of the three empirical rules. That is, the atomic size has a continuous change, and additional atomic pairs of Fe–Nb, Co–Nb, Nb–P, Nb–C and Nb–B also have large negative heats of mixing. This may lead to the formation of the unique disordered structure mentioned above, which can suppress the nucleation of the crystalline phase, make the atomic rearrangement more difficult, and increase the thermal stability of the supercooled liquid.

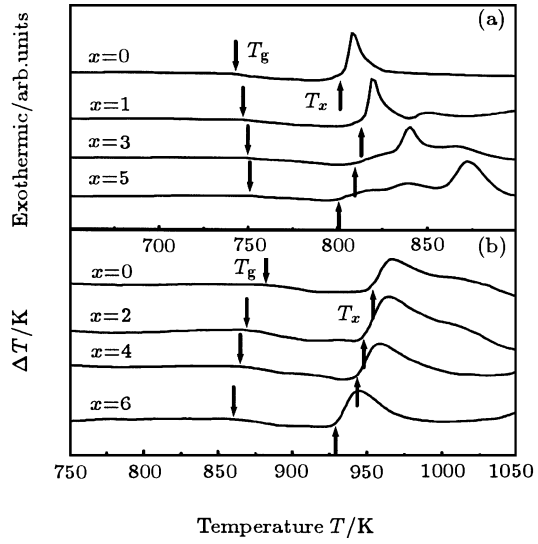


Fig.2. DSC curves of Fe_{73} $Nb_xAl_{5-x}Ge_2P_{10}C_6B_4$ alloys and DTA curves of $Fe_{63}Co_7Nb_xZr_{10-x}B_{20}$ alloys: (a) $Fe_{73}Nb_xAl_{5-x}Ge_2P_{10}C_6B_4$; (b) $Fe_{63}Co_7Nb_x$ $Zr_{10-x}B_{20}$.

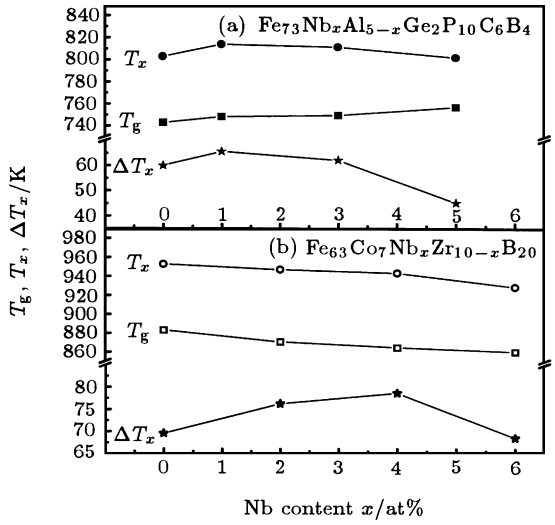


Fig.3. Changes in the glass transition temperature (T_g), onset temperature of crystallization (T_x) and temperature interval of supercooled liquid region (ΔT_x=T_x–T_g) as functions of Nb content for the amorphous $Fe_{73}Nb_xAl_{5-x}Ge_2P_{10}C_6B_4$ and $Fe_{63}Co_7Nb_xZr_{10-x}B_{20}$ alloys.

In order to investigate the effect of Nb on the supercooled liquid region ΔT_x, the melt-spun ribbons with a thickness of 100μm for $Fe_{73}Nb_x$ $Al_{5-x}Ge_2P_{10}C_6B_4$ alloys were prepared. It is well known that Nb has large negative heats of mixing against all the other constituent elements,[21] and hence Nb has a high tendency to form various kinds of compounds with other elements such as Fe_xNb_y, Nb_xAl_y, Nb_xGe_y, Nb_xP_y, Nb_xC_y and Nb_xB_y. However, we cannot detect any of these compounds for the alloys containing 0 and 1 at% Nb. This indicates the necessity of the redistribution of the Nb element from the supercooled liquid to the crystallized phases in the progress of crystallization. The redistribution is not always easy for elements with high melting temperatures, such as Nb, so the addition of Nb can lead to the retardation of precipitation of crystallized phases. The decrease in ΔT_x with further increasing Nb content is presumably due to the formation of an inhomogeneously mixed atomic configuration which is favourable for easy precipitation of the crystallized phases, as evidenced from the precipitation of NbC and Nb_3B_2, respectively, for $Fe_{73}Nb_3Al_2Ge_2P_{10}C_6B_4$ and $Fe_{73}Nb_5Ge_2P_{10}C_6B_4$ alloys (see Fig.4). That is, the effectiveness of Nb for the increase in ΔT_x seems to be obtained only at an optimum Nb content leading to the formation of a homogeneously mixed glass structure. This result is in good agreement with the thermal stability analysis in Fig.3. The above discussion can also be applied to the $Fe_{63}Co_7Nb_xZr_{10-x}B_{20}$

alloy system.

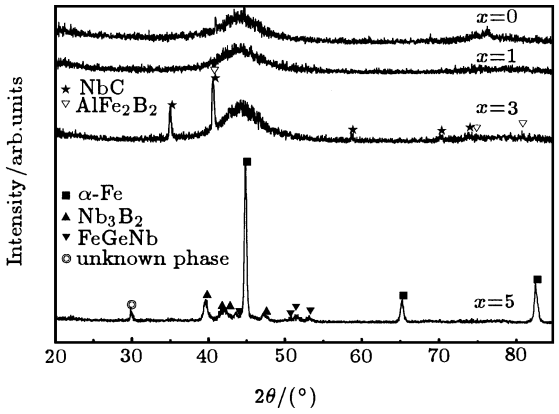


Fig.4. X-ray diffraction patterns taken from the freely solidified surfaces of 100μm thick melt-spun ribbons of $Fe_{73}Nb_xAl_{5-x}Ge_2P_{10}C_6B_4$ alloys.

3.2. Magnetic properties

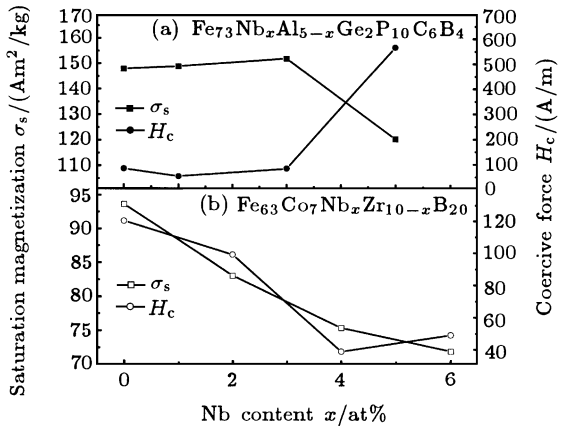


Fig.5. Saturation magnetization σ_s and coercive force H_c as functions of Nb content at room temperature for $Fe_{73}Nb_xAl_{5-x}Ge_2P_{10}C_6B_4$ and $Fe_{63}Co_7Nb_xZr_{10-x}B_{20}$ alloys.

Figure 5 shows the saturation magnetization σ_s under a field of 800kA/m and the coercive force H_c of melt-spun ribbons as functions of Nb content at room temperature for $Fe_{73}Nb_xAl_{5-x}Ge_2P_{10}C_6B_4$ and $Fe_{63}Co_7Nb_xZr_{10-x}B_{20}$ alloy series. It is seen that σ_s is near 150Am^2/kg and does not change significantly with the increase of Nb content from 0 to 3 at% for $Fe_{73}Nb_xAl_{5-x}Ge_2P_{10}C_6B_4$ alloys, but decreases rapidly to 120Am^2/kg when the Nb content increases to 5 at%. This may be due to the inhomogeneously mixed atomic configuration in the $Fe_{73}Nb_5Ge_2P_{10}C_6B_4$ alloy. But for $Fe_{63}Co_7Nb_xZr_{10-x}B_{20}$ alloys, σ_s decreases linearly from 94 to 72Am^2/kg with the increase of Nb content from 0 to 6 at% and is significantly lower than that of $Fe_{73}Nb_xAl_{5-x}Ge_2P_{10}C_6B_4$ alloys. The minimum coercive force H_c is 49 and 38A/m, respectively, for the $Fe_{73}Nb_1Al_4Ge_2P_{10}C_6B_4$ and $Fe_{63}Co_7Nb_4Zr_6B_{20}$ alloys.

In order to obtain better magnetic properties, the two alloy systems have been annealed at 573–973K for 15min in vacuum. Figure 6 shows the saturation magnetization σ_s as a function of annealing temperature T_a for the annealed ribbons of the two alloy series. It is seen that σ_s does not change significantly when the annealing temperature is below 773K, but increases in small amounts at higher annealing temperatures for the $Fe_{73}Nb_xAl_{5-x}Ge_2P_{10}C_6B_4$ alloy system, and the maximum σ_s reaches 158Am^2/kg for this alloy. As for the $Fe_{63}Co_7Nb_xZr_{10-x}B_{20}$ alloy system, σ_s is almost unchanged when the annealing temperature is below 873K and increases distinctly from 95 to 107Am^2/kg, 90 to 99Am^2/kg, 73 to 94Am^2/kg and 73 to 103Am^2/kg, respectively, for alloys containing 0, 2, 4 and 6 at% Nb annealed at 973K.

It is well known that the internal hardening stress of melt-spun ribbons is very high and the coercive force H_c can be decreased by decreasing the internal stress through relaxation or annealing at an appropriate temperature. Figure 7 shows the dependence of the coercive force H_c on annealing temperature for $Fe_{73}Nb_xAl_{5-x}Ge_2P_{10}C_6B_4$ and $Fe_{63}Co_7Nb_xZr_{10-x}B_{20}$ ribbons annealed for 15min in vacuum. H_c reaches minimum values of 62, 31, 73 and 246A/m, respectively, for 0, 1, 3 and 5 at% Nb alloys in the $Fe_{73}Nb_xAl_{5-x}Ge_2P_{10}C_6B_4$ alloy system after annealing at 773K for 15min. For the $Fe_{63}Co_7Nb_xZr_{10-x}B_{20}$ alloy system, H_c reaches minimum values of 57, 56, 37 and 44A/m, respectively, for 0, 2, 4 and 6 at% Nb alloys after annealing at 873K. However, H_c will increase distinctly when the annealing temperature is higher than the crystallization temperature of two alloy series.

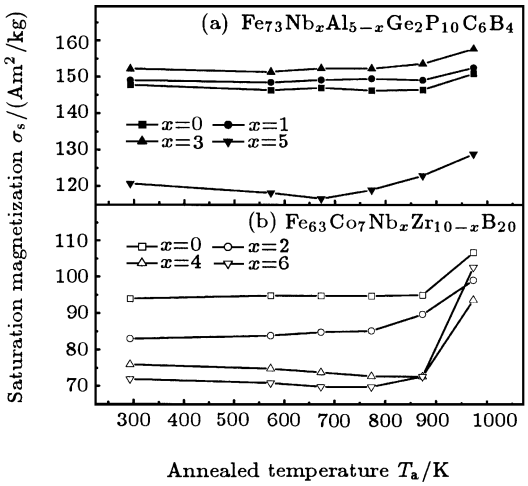


Fig.6. Saturation magnetization σ_s as a function of annealing temperature T_a for two alloy systems annealed at different temperatures for 15min in vacuum.

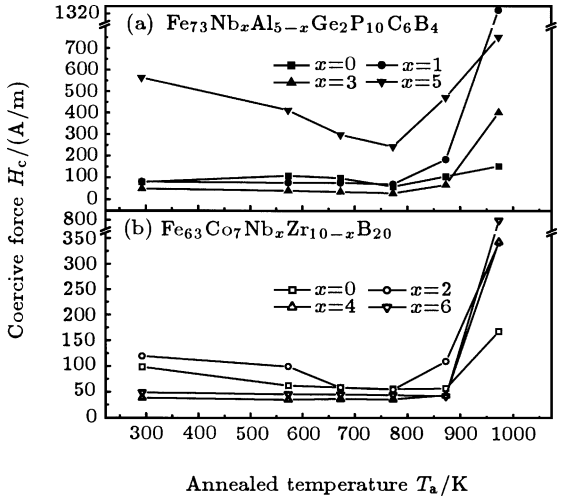


Fig.7. Coercive force H_c as a function of annealing temperature for two alloy systems annealed at different temperatures for 15min in vacuum.

The increase of σ_s and H_c of the ribbons annealed at high temperature may be due to the precipitation of crystallized phases. Figure 8 shows the X-ray diffraction patterns of $Fe_{73}Nb_1Al_4Ge_2P_{10}C_6B_4$ and $Fe_{63}Co_7Nb_4Zr_6B_{20}$ ribbons annealed at 973K for 15min in vacuum. It is seen that α-Fe, Fe_3B, FeB, Fe_3P, Fe_3C phases are precipitated in the $Fe_{73}Nb_1Al_4Ge_2P_{10}C_6B_4$ alloy and α-Fe, Fe_3Zr, ZrB_{12} phases are precipitated in the $Fe_{63}Co_7Nb_4Zr_6B_{20}$ alloy.

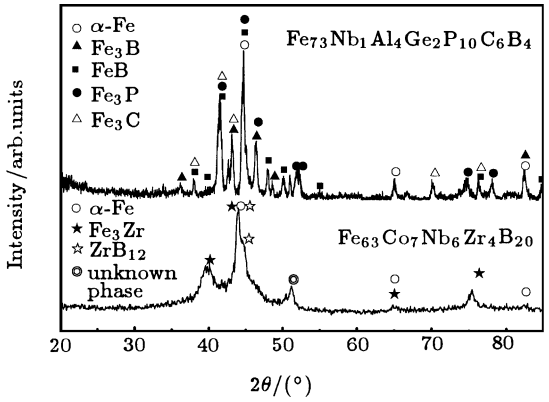


Fig.8. X-ray diffraction patterns taken from the free surfaces of $Fe_{73}Nb_1Al_4Ge_2P_{10}C_6B_4$ and $Fe_{63}Co_7Nb_4Zr_6B_{20}$ amorphous alloys annealed for 15min at 973K.

4. Conclusion

In order to find a new Fe-based amorphous alloy with an extended supercooled liquid region before crystallization and good magnetic properties, we have examined the effect of the addition of the Nb element on ΔT_x and magnetic properties for $Fe_{73}Nb_xAl_{5-x}Ge_2P_{10}C_6B_4$ (x=0, 1, 3, 5 at%) and $Fe_{63}Co_7Nb_xZr_{10-x}B_{20}$ (x=0, 2, 4, 6 at%) alloys. The results obtained are summarized as follows.

(1) ΔT_x increases with the addition of Nb, and the maximum values of 66 and 79K are obtained, respectively, for $Fe_{73}Nb_1Al_4Ge_2P_{10}C_6B_4$ and $Fe_{63}Co_7Nb_4Zr_6B_{20}$ alloys.

(2) The extension of the supercooled liquid region by the dissolution of an optimum amount is presumably due to the retardation of the redistribution of the constituent elements for the progress of crystallization.

(3) The $Fe_{73}Nb_xAl_{5-x}Ge_2P_{10}C_6B_4$ alloys have high σ_s of about 150Am^2/kg and are nearly unchanged with the increase of Nb content from 0 to 3 at%. But it decreases rapidly to 120Am^2/kg for the alloy containing 5 at% Nb. For the $Fe_{63}Co_7Nb_xZr_{10-x}B_{20}$ alloys, σ_s decreases nearly linearly from 94 to 72Am^2/kg with the decrease of Nb content. H_c obtains minimum values when the Nb content is 1 and 4 at%, respectively, for the two alloy series.

(4) σ_s is almost unchanged when the annealing temperature T_a is below 773 and 873K, respectively, for $Fe_{73}Nb_xAl_{5-x}Ge_2P_{10}C_6B_4$ and $Fe_{63}Co_7Nb_xZr_{10-x}B_{20}$ alloy systems. A further increase of T_a will lead to the increase of σ_s. The coercive force obtains minimum values for the melt-spun ribbons annealed at 773 and 883K, respectively, for two alloy series.

References

[1] Inoue A *et al* 1991 *Mater. Trans. JIM* **32** 609
[2] Inoue A *et al* 1989 *Mater. Trans. JIM* **30** 378
[3] Inoue A 1993 *Mater. Trans. JIM* **34** 351
[4] Zhang T, Inoue A and Masumoto T 1991 *Mater. Trans. JIM* **32** 1005
[5] Zhang T and Inoue A 1998 *Mater. Trans. JIM* **39** 1230
[6] Peker A and Johnson W L 1993 *Appl. Phys. Lett.* **63** 2342
[7] Xu Y H and Wang W K 1990 *Acta Phys. Sin.* **39** 555 (in Chinese)
[8] Xu Y H, Cheng H and Wang W K 1992 *Acta Phys. Sin.* **41** 1111 (in Chinese)
[9] Inoue A 1996 *Mater. Trans. JIM* **37** 181
[10] Inoue A and Nishiyama N 1997 *Mater. Trans. JIM* **38** 179
[11] Inoue A and Zhang T 1996 *Mater. Trans. JIM* **37** 185
[12] He D W *et al* 1998 *Acta Phys. Sin.* **47** 183 (in Chinese)
[13] Inoue A 1995 *Mater. Trans. JIM* **36** 866
[14] Shen T D and Schwarz R B 1999 *Appl. Phys. Lett.* **75** 49
[15] He J *et al* 1999 *Acta Phys. Sin.* (*Overseas Edition*) **8** 208
[16] Lin D M *et al* 1999 *Acta Phys. Sin.* (*Overseas Edition*) **8** 455
[17] Wang X F *et al* 2001 *Chin. Phys.* **10** 555
[18] Inoue A, Makino A and Mizushima T 1997 *J. Appl. Phys.* **81** 4029
[19] Inoue A *et al* 1997 *Mater. Trans. JIM* **38** 359
[20] Inoue A *et al* 1998 *Mater. Trans. JIM* **39** 318
[21] Miedema A R 1976 *Phil. Tech. Rev.* **36** 217